High-Gradient Magnetic Separation of Coated Magnetic Nanoparticles

Geoffrey D. Moeser, Kaitlin A. Roach, William H. Green, and T. Alan Hatton
Dept. of Chemical Engineering, Massachusetts Institute of Technology, Cambridge, MA 02139

Paul E. Laibinis
Dept. of Chemical Engineering, Rice University, Houston, TX 77005

DOI 10.1002/aic.10270
Published online in Wiley InterScience (www.interscience.wiley.com).

The feasibility is examined of using high-gradient magnetic separation (HGMS) to recover about 8-nm magnetite nanoparticles that are tailored specifically to extract target solutes (polymer-coated nanoparticles for the extraction of soluble organic contaminants from water and phospholipid-coated particles for the selective extraction of proteins). A general model for nanoparticle capture based on calculating the limit of static nanoparticle buildup around the wires in an HGMS column is presented. Model predictions are compared successfully with experimental results from a bench-scale HGMS column for both the polymer- and phospholipid-coated particles. A minimum diameter for successful particle capture is derived for both individually dispersed nanoparticles and aggregates of nanoparticles. The individually dispersed polymer-coated nanoparticles are less easily captured in the HGMS column than are the phospholipid-coated particles, which exist as submicron aggregates. © 2004 American Institute of Chemical Engineers *AIChE J,* 50: 2835–2848, 2004

Keywords: high gradient magnetic separation (HGMS), magnetic nanoparticles, magnetic fluid, organic extraction, protein separation

Introduction

High-gradient magnetic separation (HGMS) is used to separate magnetic materials from a nonmagnetic liquid medium. This process has traditionally been applied in kaolin clay benefaction, the removal of iron particles from process streams in steel and power plants, and wastewater treatment of bacteria and solids through magnetic seeding (Gerber and Birss, 1983; Ying et al., 2000). More recently, HGMS has been applied to more complex separations through the use of functionalized magnetic particles that are tailored to selectively remove cells (Safarik and Safarikova, 1999), proteins (Bucak et al., 2003; Hubbuch and Thomas, 2002), or environmental contaminants such as radionuclides (Buchholz et al., 1996), heavy metal ions (Kaminski and Nunez, 1999; Leun and Sengupta, 2000), dyes (Safarik, 1995), and nonpolar organic contaminants (Moeser et al., 2002).

An HGMS system generally consists of a column packed with a bed of magnetically susceptible wires (diameter $\sim$ 50 μm) placed inside an electromagnet. When a magnetic field is applied across the column, the wires dehomogenize the magnetic field in the column, producing large field gradients around the wires that attract magnetic particles to their surfaces and trap them there (Gerber and Birss, 1983). The collection of particles depends strongly on the creation of these large magnetic field gradients, as well as on the particle size and magnetic properties, as shown by the equation for the magnetic force on a particle in an applied field (Gerber and Birss, 1983):

$$\mathbf{F_m} = \mu_o V_p \mathbf{M_p} \cdot \nabla \mathbf{H} \quad (1)$$

Correspondence concerning this article should be addressed to A. Hatton at tahatton@mit.edu.

where μ_o is the permeability of free space, V_p is the volume of the particle, $\mathbf{M_p}$ is the magnetization of the particle, and $\mathbf{H}$ is the magnetic field at the location of the particle. For successful collection of magnetic particles by HGMS, the magnetic force attracting particles toward the wires must dominate the fluid drag, gravitational, inertial, and diffusional forces as the particle suspension flows through the separator (Gerber and Birss, 1983). Typically, HGMS has been used to separate micron-scale or larger particles or aggregates. In some cases, magnetic nanoparticles have been used as separation agents; however, these nanoparticles have usually been present as micron-scale aggregates (Hubbuch and Thomas, 2002) or encapsulated into larger polymer beads (Leun and Sengupta, 2000). The larger volume of these particles makes magnetic collection by HGMS (or other means) relatively straightforward. The application of HGMS to suspensions of individually dispersed magnetic nanoparticles (magnetic fluids) has been studied in much less depth.

Magnetic fluids are colloidal dispersions of magnetic nanoparticles that do not settle under gravitational and moderate magnetic fields because of their small size (~10 nm) and do not aggregate because of their surface coatings (Rosensweig, 1985). Recently, we synthesized water-based magnetic fluids with coatings that are tailored both to provide colloidal stability in the dispersion medium and to have an affinity for a particular target solute, so they could be used as HGMS separation agents for small organic molecules (Moeser, 2003; Moeser et al., 2002) or proteins (Bucak et al., 2003). Our magnetic fluids for separating organic compounds from water consist of stable suspensions of magnetite (Fe_3O_4) nanoparticles coated with a bifunctional polymer layer that is composed of an outer hydrophilic polyethylene oxide (PEO) region for colloidal stability in the dispersion medium (water) and an inner hydrophobic polypropylene oxide (PPO) region for solubilization of organic compounds (Moeser et al., 2002). Previous studies have shown that these nanoparticles have a high affinity for nonpolar organics, with partition coefficients on the order of 10^3 to 10^5 between the hydrophobic region and water (Moeser, 2003; Moeser et al., 2002). The magnetic fluids for protein separation consist of magnetite nanoparticles coated with a surfactant-phospholipid bilayer that provides both electrostatic stabilization in water and high affinity for many hydrophilic proteins (Bucak et al., 2003). In both systems, the magnetic fluids have many advantages over traditional fixed-bed separation methods, such as activated carbon adsorption for organics and affinity chromatography for proteins. In particular, the magnetic nanoparticles offer large exposed surface areas without the use of porous materials, which are often plagued by high mass transfer resistances. In addition, HGMS can potentially allow direct processing of streams with suspended solids, in contrast to most traditional separation methods that can be fouled by the presence of these large contaminants.

Figure 1 shows how these magnetic fluids could be integrated into a practical separation process. In the contacting stage, a concentrated suspension of the nanoparticles is mixed with the process stream, which is contaminated water for the polymer-coated particles or a fermentation mixture for the phospholipid-coated particles. After the particles are loaded with the target solute, they are trapped in the HGMS column, leaving either purified water (polymer-coated particles) or unwanted biomass (phospholipid-coated particles) as the effluent.

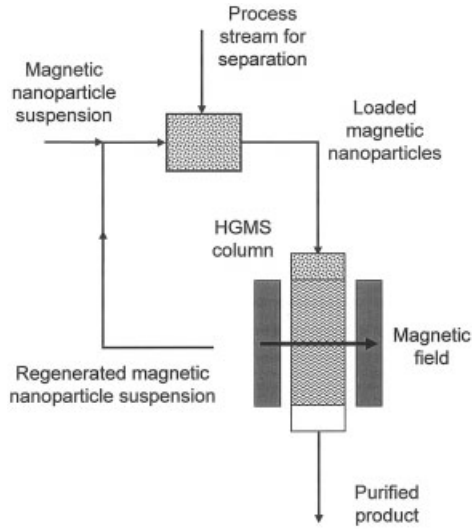

Figure 1. A generalized process using functionalized magnetic nanoparticles as separation agents.

After contact with a process stream containing the target solute, the loaded particles are removed with HGMS. A magnetic field is applied across the column, generating magnetic field gradients in the liquid around the wires that trap the particles in the column. After regeneration, the nanoparticles can be recycled to the contacting stage.

This process obviously requires that the HGMS column efficiently remove the magnetic nanoparticles from the dispersion medium. Although some work has been performed using HGMS to separate individually dispersed magnetic nanoparticles, the majority of this work has been theoretical and limited to simulating the behavior of nanoparticles around a single HGMS wire (Fletcher, 1991; Gerber et al., 1983; Takayasu et al., 1983) or sphere (Cotten and Eldredge, 2002; Ebner et al., 1997; Moyer et al., 1984). These simulations suggest that the collection of magnetic nanoparticles by HGMS is possible but the small size of the particles presents challenges not associated with larger particles. Recently, theoretical predictions of submicron particle capture have been compared with experimental results, but these studies have focused on particles greater than 100 nm where diffusion is a secondary effect (Ying et al., 2000).

Our preliminary results have shown that, although HGMS can be applied successfully to the phospholipid-coated particles for protein separation (Bucak et al., 2003), the polymer-coated particles for organic removal are more difficult to capture (Moeser, 2003; Moeser et al., 2002). In this article, we present a study on the use of HGMS to separate magnetic nanoparticles and nanoparticle aggregates from water by measuring the capture efficiency of our magnetic fluids in a bench-scale HGMS system. We also develop a model for the specific geometry of our HGMS column whose predictions agree with the experimental results and reveal the important forces that act on nanoparticles during the HGMS process. In particular, we observe a strong dependency of the capture efficiency on particle size. From these results, we can draw conclusions about the feasibility of HGMS for different classes of magnetic fluids and develop guidelines for optimization of the polymer-coated nanoparticles for effective use in chemical processing applications.

Experimental

Materials

Polyacrylic acid (50 wt % in water, M_w = 5000), iron (III) chloride hexahydrate (97%), iron (II) chloride tetrahydrate (99%), ammonium hydroxide (28 wt % in water), hydrochloric acid (37 wt % in water), decanoic acid, Tiron (4,5-dihydroxy-1,3-benzene-disulfonic acid, disodium salt monohydrate), and TES buffer (*N*-tris [hydroxymethyl] methyl-2-aminoethanesulfonic acid) were obtained from Sigma–Aldrich (Milwaukee, WI). Jeffamine XTJ-234 (CH_3–O–PEO/PPO–NH_2, EO:PO = 6.1:1, M_w = 3000) was a gift from Huntsman Corp. (Houston, TX). Herein, we consider XTJ-234 to be equivalent to pure PEO and we refer to this polymer as PEO–NH_2. DMPG (1,2-myristoyl-*sn*-glycero-3-phosphocholine) was provided by Genzyme Pharmaceuticals (Cambridge, MA). All chemicals were used as received.

Synthetic procedure

Detailed descriptions of the synthetic procedures for the polymer-coated (Moeser, 2003; Moeser et al., 2002) and phospholipid-coated (Bucak et al., 2003) magnetic fluids are given in previous publications. In summary, the graft copolymer for the polymer-coated particles was synthesized by reacting polyacrylic acid (PAA) with PEO-NH_2. The stoichiometry of this reaction was selected so that 16% of the carboxylic acid groups on the PAA backbone were substituted with PEO-NH_2 side chains. The polymer-coated nanoparticles were then produced by coprecipitation of iron (II) and iron (III) chloride to form magnetite in the presence of this graft copolymer. The phospholipid-coated particles were synthesized by coprecipitation of iron (II) and iron (III) chloride in the presence of decanoic acid to form decanoic acid bilayer–coated magnetite nanoparticles. The outer layer of decanoic acid around the nanoparticles was then exchanged with DMPG phospholipid by dialysis to produce the phospholipid-coated nanoparticles. In both magnetic fluid syntheses, nanoparticles are formed because the polymer or surfactant binds to the magnetite surface just after particle nucleation, thereby limiting particle growth.

Magnetic filtration and chromatography

HGMS experiments were performed with a Model L-1CN Frantz Canister Separator (S.G. Frantz Co., Trenton, NJ). The HGMS system consisted of a cylindrical glass column with an internal radius of 0.285 cm and a length of 22.6 cm (a volume of 5.77 cm^3) that was randomly packed with 6.2 g of type 430 fine-grade stainless steel wool (40–66 μm diameter), also supplied by S.G. Frantz. The packing occupied 0.79 cm^3, resulting in a packing fraction of 14%, which is the maximum packing fraction that could be obtained by hand. For filtration, the column was placed in a 1-cm gap between two metal plates of the separator. A variable-strength magnetic field perpendicular to the direction of flow through the column was generated between the two plates using an electromagnet. The maximum flux density of 1.3 T, as measured with a handheld magnetometer, was used in all experiments, with $\pm$3% variations resulting from temperature variations in the electromagnet.

Batch-filtration experiments were performed at room temperature by introducing 4.5 mL of dilute magnetic fluid (0.25 wt % Fe_3O_4) to the column with the electromagnet on, and then flushing the fluid from the column with air. The concentration of particles in the recovered fluid was measured by iron titration, which was performed by adding concentrated hydrochloric acid to dissolve the Fe_3O_4 particles and then titrating the resulting Fe^{3+} ions with 4,5-dihydroxy-1,3-benzene-disulfonic acid, disodium salt monohydrate (Yoe and Jones, 1944). The fraction of trapped particles was determined by difference. When the electromagnet was turned off, 4.5 mL of water was passed through the column to collect and resuspend the trapped particles. To remove any remaining particles, the column was backflushed with clean water and acetone; it was subsequently dried with a heat gun.

In the second type of HGMS experiment, referred to as magnetic chromatography, water was pumped steadily through the HGMS column with the magnet on. A 0.5-mL sample of dilute magnetic fluid was then injected with a syringe into tubing directly above the HGMS filter and the HGMS column effluent collected in 1-min batches (for high flow rates, the effluent was collected more frequently). The Fe_3O_4 particle concentration in these effluent samples was determined by measuring the turbidity at 365 nm with a Hewlett–Packard 8453 UV–visible spectrometer.

Particle characterization

Dynamic light scattering (DLS) experiments were performed with a Brookhaven BI-200SM light scattering system at a measurement angle of 90°. The autocorrelation function was fit with an exponential-fitting software program to extract the diffusion coefficient, and the Stokes–Einstein equation was used to convert the diffusion coefficient to the hydrodynamic diameter. Intensity-average size distributions provided by the light scattering software were converted to volume-average and number-average size distributions for further analysis. Quoted particle sizes are the average of five measurements. All samples were filtered with a 0.22-μm syringe filter to remove dust. Zeta potential results were obtained using a Brookhaven ZetaPals Zeta Potential Analyzer.

HGMS Modeling

High-gradient magnetic separation of micron-size particles has been modeled extensively by considering the important forces on the magnetic particles as they flow through the separator (Ebner and Ritter, 2001; Gerber and Birss, 1983; Ying et al., 2000). Particle capture has been shown to be governed by competition between the magnetic attraction of the particles to the magnetized wires and the viscous drag on the particles from the flowing fluid. When the diameter of the magnetic particles is below about 40 nm (for magnetite particles), diffusion of the particles away from the wires also becomes important (Gerber et al., 1983), and is commonly viewed as an additional force that is exerted on the nanoparticles (Fletcher, 1991).

The HGMS collection process is illustrated schematically in Figure 2. We consider a magnetically susceptible wire of radius a coated with a static nanoparticle buildup of radius b. The wire and particle buildup are surrounded by water, with a magnetic nanoparticle located at a distance r and angle θ from the wire. The illustrated orientation of the wire in Figure 2 is reasonable to consider, given that the wires in the column are generally

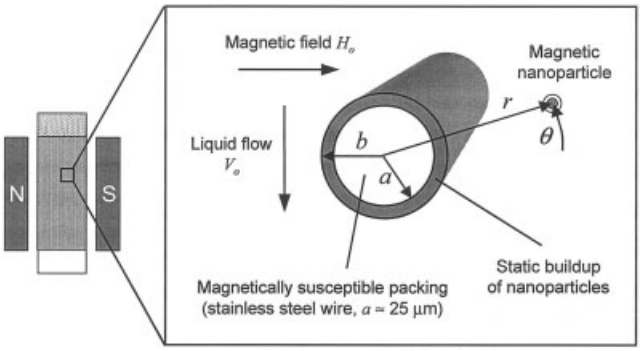

Figure 2. The HGMS model system is based on an isolated magnetically susceptible wire magnetized perpendicular to its axis, in a flow field oriented perpendicular to both the wire axis and the magnetic field.

The wire is coated with a dense static buildup of nanoparticles. A coated magnetic nanoparticle is shown at a distance r and polar angle θ from the wire center.

oriented in a direction perpendicular to the direction of fluid flow. Our assumption that the wires are also perpendicular to the applied magnetic field can be justified by noting that only wires oriented in this direction will induce magnetic field gradients; wires oriented parallel to the applied field will not induce field gradients in the liquid (Wangsness, 1979) and are considered to be dead space in the column. The motion of the nanoparticle in Figure 2 is governed by the magnetic, fluid drag, and diffusive forces exerted on it. Rather than deriving the trajectory of any given nanoparticle, in this work we consider the static balance of these forces to calculate the region around the wire where the nanoparticles can form a stable buildup (Fletcher, 1991). The size and shape of the buildup region give an indication of the effect of various parameters on HGMS.

The model we develop here for HGMS is based on the work of Fletcher (1991) with five key differences. First, as shown in Figure 2, the fluid flow is taken to be perpendicular to the direction of the applied magnetic field, in contrast to Fletcher's assumption that the flow and field directions are parallel. Second, Fletcher's theory was derived for the collection of paramagnetic nanoparticles (where the particle magnetization is a linear function of the applied field), whereas our magnetite nanoparticles are superparamagnetic (Moeser, 2003; Moeser et al., 2002). In addition, our particles are coated with a nonmagnetic polymer or phospholipid layer, as opposed to the bare magnetic particles considered by Fletcher. Therefore, although the magnetic force acts only on the magnetic core, as in Fletcher's model, we must account for the fact that the fluid drag force acts on the entire particle including the shell. In addition, our model uses a low Reynolds number solution for liquid flow around the cylindrical wire (Gerber and Birss, 1983; Ying et al., 2000), which is more applicable than the high Reynolds number solution used in Fletcher's model because the Reynolds number (based on the wire diameter) is usually less than unity for HGMS of nanoparticles. Finally, based on our zeta potential measurements and theoretical estimates of electrostatic interactions between the charged nanoparticles, we ignore these relatively weak interactions in our calculations of the static buildup regions.

The first force we consider is the fluid drag force acting on a particle in the flow field around the wire. Although there is no simple analytical solution for low Reynolds number flow around a cylinder, in the region near the surface, the velocity components of the fluid flow around the wire coated with a dense buildup of particles can be approximated by (Ying et al., 2000)

$$V_r = -V_o G^- \sin\theta \tag{2}$$

$$V_\theta = -V_o G^+ \cos\theta \tag{3}$$

where G is a geometric factor given by

$$G^\pm = \frac{\ln(r/b) \pm 0.5[1-(b/r)^2]}{2 - \ln \mathrm{Re}_b} \tag{4}$$

In this equation, Re_b is the Reynolds number based on b

$$\mathrm{Re}_b = \frac{2b\rho V_o}{\eta} \tag{5}$$

where ρ and η are the fluid density and viscosity, respectively. With this fluid velocity profile, the radial and azimuthal fluid drag force components on a nanoparticle in the fluid are given by

$$F_{vr} = -6\pi\eta R_{shell}\left(\frac{dr}{dt} + V_o G^- \sin\theta\right) \tag{6}$$

$$F_{v\theta} = -6\pi\eta R_{shell}\left(r\frac{d\theta}{dt} + V_o G^+ \cos\theta\right) \tag{7}$$

where R_{shell} is the total nanoparticle radius including the coating. In these equations, the sums in the brackets represent the motion of the particle relative to the fluid.

Particle diffusion can be described as a driving force that arises from a gradient in particle concentration. If n is defined as the particle number concentration at r and θ, then the diffusive "force" acting on particles around the wire can be written as (Fletcher, 1991)

$$F_{dr} = -\frac{kT}{n}\frac{dn}{dr} \tag{8}$$

$$F_{d\theta} = -\frac{kT}{n}\frac{1}{r}\frac{dn}{d\theta} \tag{9}$$

We assume that nanoparticles in the dense static buildup around the wire are frozen in place and unable to diffuse, but particles outside this buildup are subject to diffusional forces.

The magnetic force on the particle is determined by first solving for the magnetic field, $\mathbf{H}(r, \theta)$, that is induced in the liquid by the presence of a wire with the geometry shown in Figure 2 (Fletcher, 1991; Gerber and Birss, 1983)

$$H_r = \left(\frac{M_{wire}a^2}{2r^2} + H_o\right)\cos\theta \tag{10}$$

$$H_\theta = \left(\frac{M_{wire}a^2}{2r^2} - H_o\right)\sin\theta \tag{11}$$

In these equations, H_o is the externally applied magnetic field and M_{wire} is the magnetization of the wire. The magnetic force on a particle is then calculated from the magnetic field using Eq. 1. This result (for our wire geometry) was previously derived for paramagnetic particles, in which the particle magnetization is a linear function of the local magnetic field, $\mathbf{M_p} = \boldsymbol{\chi}\mathbf{H}$ (Fletcher, 1991; Gerber and Birss, 1983). Here, our magnetite nanoparticles are intrinsically superparamagnetic (Bucak et al., 2003; Moeser, 2003; Moeser et al., 2002), meaning that the Fe_3O_4 core magnetization, $\mathbf{M_{core}}$, is described by a Langevin function of the magnetic field (Rosensweig, 1985). However, at magnetic fields greater than approximately 1 T, as are encountered in our HMGS column, the particle cores become magnetically saturated and the core magnetization effectively attains a constant value. With these saturation conditions, the core magnetization is a vector of constant magnitude M_{core} in the direction of the magnetic field

$$\mathbf{M_{core}} = M_{core}\frac{\mathbf{H}}{|\mathbf{H}|} \tag{12}$$

If the magnitude of the magnetic field in the liquid, $|\mathbf{H}|$, is approximately equal to the applied magnetic field, H_o, then the core magnetization can be approximated as

$$\mathbf{M_{core}} \approx \frac{M_{core}}{H_o}\mathbf{H} \tag{13}$$

With this approximation, we can use the solution for paramagnetic nanoparticles (Fletcher, 1991; Gerber and Birss, 1983) by substituting $\chi = M_{core}/H_o$; this approach was previously used to simplify problems for superparamagnetic particles (Takayasu et al., 1983). The magnetic force components on a nanoparticle are therefore given by

$$F_{mr} = -\frac{4\pi\mu_o M_{wire}M_{core}a^2R_{core}^3}{3r^3}\left(\frac{M_{wire}a^2}{2H_or^2} + \cos 2\theta\right) \tag{14}$$

$$F_{m\theta} = -\frac{4\pi\mu_o M_{wire}M_{core}a^2R_{core}^3}{3r^3}\sin 2\theta \tag{15}$$

where R_{core} is the core radius of the magnetic nanoparticle.

The movement of a nanoparticle in the vicinity of the magnetized collection wire is determined by the force balance $\mathbf{F_v} + \mathbf{F_d} + \mathbf{F_m} = 0$. We have neglected inertia (the acceleration term) because of the small particle size. Balancing the radial and azimuthal force components (Eqs. 6–9, 14, 15), making the equations nondimensional by substituting $r_a = r/a$, and rearranging, we obtain the following equations for the nanoparticle trajectory in the fluid near the static buildup:

$$\frac{dr_a}{dt} = -\tau_v G^-\sin\theta - \tau_d\frac{1}{n}\frac{dn}{dr_a} - \tau_m\left(\frac{M_{wire}}{2H_or_a^5} + \frac{\cos 2\theta}{r_a^3}\right) \tag{16}$$

$$r_a\frac{d\theta}{dt} = -\tau_v G^+\cos\theta - \tau_d\frac{1}{r_a n}\frac{dn}{d\theta} - \tau_m\frac{\sin 2\theta}{r_a^3} \tag{17}$$

where τ_v, τ_d, and τ_m are constants associated with the fluid drag force, diffusion, and magnetic force, respectively

$$\tau_v = \frac{V_o}{a} \tag{18}$$

$$\tau_d = \frac{kT}{6\pi\eta R_{shell}a^2} \tag{19}$$

$$\tau_m = \frac{2\mu_o M_{wire}M_{core}R_{core}^3}{9\eta R_{shell}a^2} \tag{20}$$

Although these constants reflect the rates of particle transport by these processes, they cannot be compared directly to give a measure of the relative importance of these forces, however, because G^- and G^+ are not necessarily of order unity in Eqs. 16 and 17.

We follow the methodology of Fletcher (1991) and use Eqs. 16 and 17 to determine the outer limit of static buildup of nanoparticles around the wires (defined as b_L). This limit is the outermost point at which a particle is motionless at the interface between the static buildup and the liquid, and is reached when $dr_a/dt = 0$ and $d\theta/dt = 0$ at $r = b \equiv b_L$, or in dimensionless variables, $r_a = b/a \equiv b_{La}$. In evaluating G^- and G^+ (the geometric factors from the velocity profile), we use $r = b + R_{shell}$, because the particle center of mass can approach no closer than R_{shell} to the static buildup interface. The geometric factors for a particle sitting on the static buildup interface are therefore

$$G_b^{\pm} = \frac{\ln\left(\frac{b + R_{shell}}{b}\right) \pm 0.5\left[1 - \left(\frac{b}{b + R_{shell}}\right)^2\right]}{2 - \ln \mathrm{Re}_b} \tag{21}$$

Given that $R_{shell} \ll b$ for nanoparticles, a Taylor series expansion for both terms in the numerator yields

$$G_b^- = 0 \qquad G_b^+ = \frac{2R_{shell}/b}{2 - \ln \mathrm{Re}_b} \tag{22}$$

The limit of static nanoparticle buildup is found by substituting the limiting conditions in Eqs. 16 and 17. Following Fletcher (1991), we derive the static buildup limit for two limiting cases in which particle capture is either purely diffusion limited or purely drag force limited. For the diffusion limit of static buildup, we make the additional assumption that $V_o = 0$ (that is, a stagnant fluid). Making these substitutions in the radial force balance (Eq. 16) and integrating the term dn/dr_a with the boundary condition that $n = n_o$ when $r_a = \infty$, we obtain the nanoparticle concentration profile in a stagnant liquid as follows

$$n = n_o \exp\left[\frac{\tau_m}{2\tau_d}\left(\frac{M_{wire}}{4H_o r_a^4} + \frac{\cos 2\theta}{r_a^2}\right)\right] \tag{23}$$

Neglecting the higher-order term and making the substitution that $n = n_s$ (the number density of the static buildup of densely packed particles) at $r_a = b_{La}$, we obtain the dimensionless limit of static buildup in the purely diffusion-limited case

$$b_{La} = \left[\frac{\tau_m}{\tau_d}\frac{\cos 2\theta}{2\ln(n_s/n_o)}\right]^{1/2} \tag{24}$$

This result is identical to that obtained by Fletcher (1991). In this equation, n_s can be estimated by assuming simple cubic packing in the dense static buildup of particles, where $n_s = 1/(2R_{shell})^3$ (Fletcher, 1991). We could also have derived Eq. 24 from the azimuthal force balance with the same assumptions.

The limit of static buildup in a purely drag force–limited case is found with the additional assumption that $dn/dr_a = dn/d\theta = 0$ (that is, no diffusion). The radial force balance does not yield a limit, given that $G_b^- = 0$, but the azimuthal force balance does, and the dimensionless limit of static buildup in the purely drag force-limited case is found to be

$$\frac{b_{La}^2}{2 - \ln \mathrm{Re} - \ln b_{La}} = -\frac{\tau_m}{\tau_v}\frac{a}{R_{shell}}\sin\theta \tag{25}$$

This is a new result for low Reynolds number flow (with the geometry shown in Figure 2) that must be solved numerically for b_{La}. In this equation, we have factored b_{La} from Re_b, leaving the traditional Reynolds number Re based on a

$$\mathrm{Re} = \frac{2a\rho V_o}{\eta} \tag{26}$$

The actual limit of static buildup of particles around the wire is defined as the region in which both diffusion and fluid drag on the particle are overcome by the magnetic force. This region is defined by the intersection of the areas inside both the diffusion and drag force buildup limits given by Eqs. 24 and 25, respectively (Fletcher, 1991). These equations also yield dimensionless quantities showing the relative importance of the individual forces acting on the nanoparticles in the HGMS column. The diffusion limit is dependent on the dimensionless variable $K_{md} \equiv \tau_m/\tau_d$, which gives the ratio of the magnetic force to the diffusive force

$$K_{md} = \frac{\tau_m}{\tau_d} = \frac{4\pi\mu_o M_{wire} M_{core} R_{core}^3}{3kT} \tag{27}$$

This ratio approaches unity when the forces are similar in magnitude.

The quantity τ_m/τ_v (or V_m/V_o using conventional nomenclature) is often used as a measure of the importance of the magnetic force relative to the drag force, but this is not a useful metric in this case because $\tau_m/\tau_v \ll 1$ when the forces are close in magnitude. Our derivation (Eq. 25) indicates that this ratio should be mulitiplied by a/R_{shell} ($\gg$1 for nanoparticles) to account for the fact that the fluid velocity near the edge of the buildup, which determines whether a particle is captured statically, is much lower than it is far from the wire. Thus the ratio

$$K_{mv} = \frac{\tau_m}{\tau_v}\frac{a}{R_{shell}} = \frac{2\mu_o M_{wire} M_{core} R_{core}^3}{9\eta R_{shell}^2 V_o} \tag{28}$$

gives a better estimate of the relative importance of these forces near the wire or static buildup than does τ_m/τ_v itself.

This model for HGMS yields the limit of static buildup of nanoparticles around the magnetized collection wires and can be used to reconcile our bench-scale experimental results.

Results and Discussion

HGMS of polymer-coated nanoparticles

The polymer-coated nanoparticles designed to separate soluble organic compounds from water consist of a magnetite (Fe_3O_4) core coated with a graft copolymer consisting of a polyacrylic acid backbone with grafted polyethylene oxide (PEO) and polypropylene oxide (PPO) side chains. This polymer forms a shell with an outer hydrophilic PEO region for stabilization in water and an inner hydrophobic PPO region for organic solubilization (Moeser, 2003; Moeser et al., 2002). These particles have been characterized by transmission electron microscopy (TEM), magnetization curve analysis, and DLS (Moeser et al., 2002). Figure 3 summarizes the results for nanoparticles stabilized with a graft copolymer containing only PEO side chains. In this work, we focus on these particles because they are similar in both their dimensions and HGMS performance to nanoparticles that include hydrophobic PPO side chains (for organic solubilization) (Moeser et al., 2002). The Fe_3O_4 cores of the particles exhibited a lognormal size distribution with a median core diameter, D_{core}, of 7.5 nm with a σ value of 0.32 (Figure 3a). In Figure 3b, the magnetization response of the magnetic fluid at two concentrations shows that the particle suspensions are superparamagnetic, given that they become magnetically saturated at high applied fields and show essentially no remanence. The saturation magnetization of the Fe_3O_4 core, M_{core}, is 63 $\pm$ 5 emu/g, which is less than the literature value for bulk magnetite of 87 emu/g, probably because the electronic structure of the outer layer of iron atoms is disrupted (Feltin and Pileni, 1997; Shen et al., 1999). Dynamic light scattering (Figure 3c) yielded an average hydrodynamic diameter, D_{shell}, of 26 nm for the particles. The DLS volume-average size distribution for the particles in Figure 3c illustrates that the distribution consisted primarily of individual particles, although larger aggregates approximately 60 to 125 nm in diameter were also present. Figure 3d provides a summary illustration of the average particle dimensions.

Small volumes of these graft copolymer–based magnetic fluids could be passed through the HGMS column with approximately 90% particle retention (Moeser et al., 2002). The captured particles were recovered by turning off the magnet and flushing the column with a given volume of fresh water. The suspension thus obtained was fed to the column again. After three such passes through the HGMS column, the smallest particles were removed and the capture efficiency of the remaining particles approached 98%. This limiting recovery was observed in all subsequent passes of the recovered particle suspension through the filter, and complete recovery of the

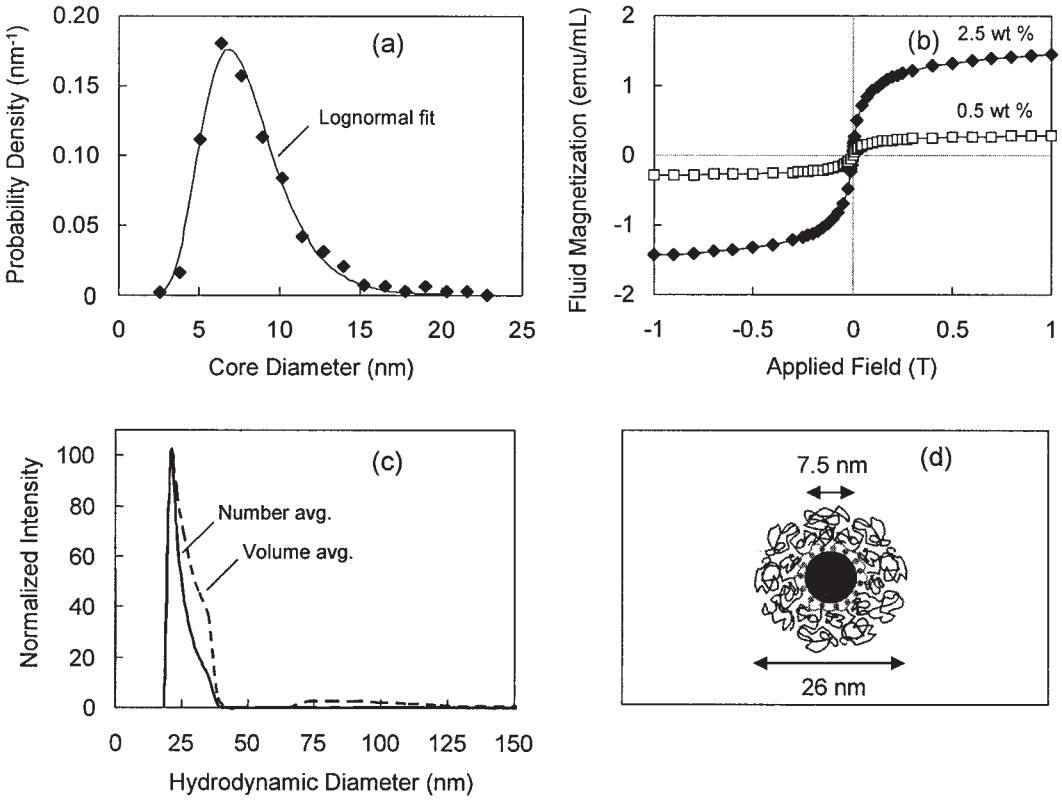

Figure 3. Overview of characterization of the polymer-coated particles (Moeser et al., 2002).

(a) The size distribution of the Fe_3O_4 core from TEM has a median core diameter (D_{core}) of 7.5 nm. (b) The magnetization as a function of the applied field strength gives a saturation magnetization of the Fe_3O_4 core (M_{core}) of 63 emu/g. (c) The hydrodynamic diameter from DLS shows two populations—individual particles with an average diameter of 26 nm (D_{shell}), and aggregates that are 60–125 nm in diameter. (d) A summary of the average nanoparticle dimensions.

particles was never achieved (Moeser et al., 2002). Variations in the particle concentration did not affect the relative fraction of particles lost in the filtrate, possibly reflecting the effect of bulk concentration on the static buildup volume, and hence on particle removal from the suspension, which increases with increasing n_o as predicted by Eq. 24. The inability to capture particles with 100% efficiency in these experiments is probably indicative of the dynamic equilibrium established between particles in the static buildup volume and the bulk solution. In a practical separation process, the HGMS column would need to process much larger volumes of magnetic fluid with significantly lower particle losses.

The effect of flow velocity on particle capture in a batch HGMS filtration of 4.5 mL of magnetic fluid is shown in Figure 4a. At low flow velocities (near 0.1 cm/s, the value used in the experiments referred to above), the effect was small, given that the velocity could be increased or decreased by nearly an order of magnitude with less than 10% change in filtration performance. In contrast, above about 1 cm/s, the fraction of particles lost in the filtrate increased dramatically. Thus, the HGMS collection of these nanoparticles can be divided into two regimes: a high-velocity regime in which fluid drag is the primary force competing against the magnetic force of attraction toward the wires, and a low-velocity regime in which the magnetic force competes primarily with particle diffusion and fluid drag is relatively unimportant. These regimes reflect the dimensionless force ratios K_{md} and K_{mv}, which were calculated for our particles using standard values of ρ and η for water, our average measured values of R_{core} (3.75 nm) and R_{shell} (13 nm) for the individual nanoparticle dimensions (Figure 3d), and the nominal radius of the wires for a (25 μm). The saturation magnetization of the Fe_3O_4 nanoparticles (Figure 3b) was used for M_{core} (63 emu/g) and the literature value of the saturation magnetization of stainless steel was used for M_{wire} (153 emu/g) because the applied magnetic field in the column (1.3 T) was sufficient to saturate both materials (Gerber and Birss, 1983). The variation of the calculated force ratios with flow velocity is shown in Figure 4b, which illustrates that at high flow velocities, K_{mv} is small and the drag force is limiting. As the flow velocity is reduced, K_{mv} becomes large and below about 0.1 cm/s, K_{md} dominates particle retention. Because K_{md} does not depend on V_o, the flow velocity no longer has an effect on the HGMS collection efficiency, as was observed experimentally in Figure 4a. This result was also predicted theoretically by Fletcher (1991).

The diffusion and drag force limits of static particle buildup given by Eqs. 24 and 25 are shown in Figure 5a for the five flow velocities shown in Figure 4a. The number densities n_s and n_o were calculated using simple cubic packing and the initial magnetite concentration, respectively, yielding n_s/n_o = 24.0 for the average nanoparticles shown in Figure 3d. The diffusion buildup limit for this analysis is independent of the flow velocity, whereas the drag force buildup limit increases in size with decreasing velocity, as the fluid drag force on the

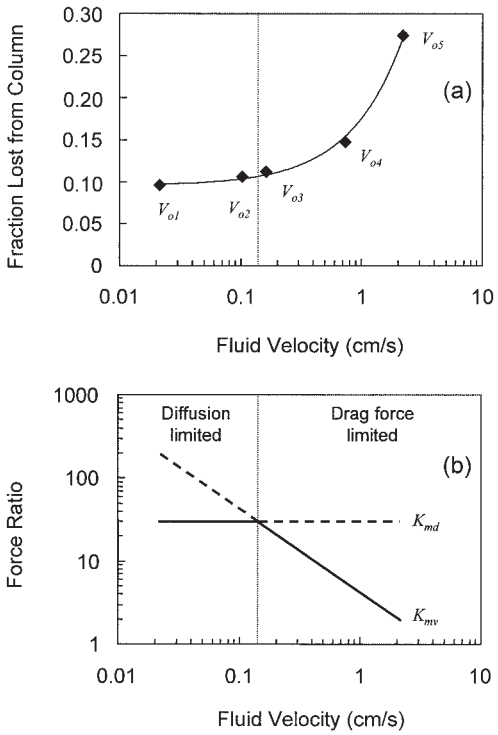

Figure 4. (a) Effect of flow velocity on batch HGMS capture of the polymer-coated nanoparticles. In this experiment, 4.5 mL of magnetic fluid was passed through the HGMS column (void volume = 5.0 mL) at various flow velocities (V_o) (the concentration of particles lost in the filtrate was measured and normalized by the initial concentration); (b) effect of flow velocity on the dimensionless ratios expressing the ratio of the magnetic force to the diffusive (K_{md}) and fluid drag (K_{mv}) forces.

The transition velocity between diffusion- and drag force-limited HGMS collection is approximated by the intersection of these two lines, with the limiting ratio shown as a solid line.

particle is overcome by the magnetic force at increasing distances. The area of overlap of the two profiles represents the region where the polymer-coated nanoparticles can be statically trapped. For V_{o1}, V_{o2}, and V_{o3} ($V_o \leq 0.2$ cm/s), the drag force buildup limit is sufficiently large that diffusion dominates particle collection, in that the total buildup volume is independent of the flow velocity. However, for V_{o4} and V_{o5} ($V_o \geq 0.7$ cm/s), the fluid drag force becomes limiting because the region of static buildup decreases in size as the outer part of the diffusion limit is eroded. The theoretically predicted transition velocity between the two regimes ($V_{o3} \rightarrow V_{o4}$) is consistent with the experimental data in Figure 4a. In addition, this transition velocity is similar to that obtained from the order of magnitude analysis of K_{md} and K_{mv} in Figure 4b.

When the magnetic field is applied perpendicular to the direction of fluid flow (as in our HGMS column), static particle capture is possible only in the two regions below the wire where the radial component of the magnetic force acts toward the wire center and the azimuthal component of the magnetic force acts in the upstream direction. Above the wire, the azimuthal component of the magnetic force acts in the same direction as the fluid flow and capture is not possible. Turbulent flow that might cause eddies below the wire is not a concern for the velocities used here because the Reynolds number is less than or equal to unity for all five flow velocities. When the fluid flow is parallel to the applied magnetic field, the diffusion buildup limit (Eq. 24) is unchanged, whereas the drag force buildup limit (Eq. 25) is modified by changing $\sin\theta$ to $-\cos\theta$. As shown in Figure 5b, the predicted result of rotating the fluid flow direction by $-90°$ is a rotation of the drag force buildup limit by 90°. Although it may appear counterintuitive, capture occurs on the upstream half of the wire when the fluid flow is parallel to the applied field, as has been noted before by Fletcher (1991). In addition, the transition velocity between the two HGMS regimes is higher in this configuration, as capture at V_{o4} becomes limited entirely by the diffusion-limited lobe. In the diffusion-limited regime, the fluid flow direction should have no effect on HGMS efficiency, given that the total static buildup volume remains the same (that is, the downstream halves of the two lobes in Figure 5a and the upstream lobe in Figure 5b).

The most important difference between our model and that of Fletcher (1991) is in the functional form of the drag force buildup limit, attributed to our use of a velocity profile that is more appropriate for low Reynolds number flow, in contrast to

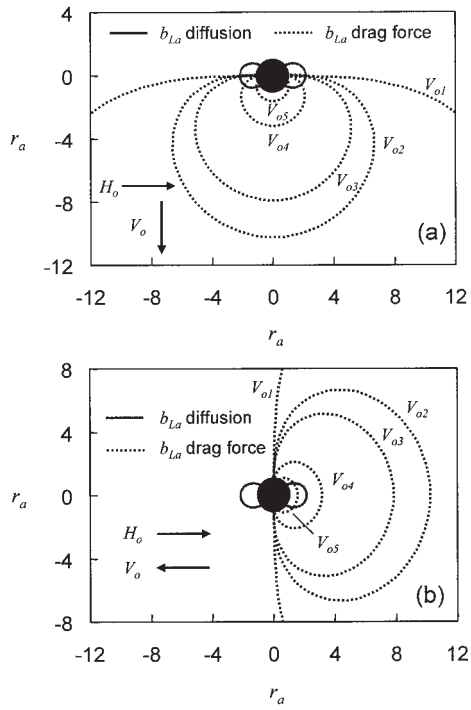

Figure 5. Predicted diffusion (solid line) and fluid drag (dotted line) force limits of static buildup for polymer-coated nanoparticles.

The actual limit of static buildup at a given flow velocity is defined by the intersection of the areas inside the diffusion- and drag force-limited curves. The circle represents the cylindrical wire and the dimensionless distance (r_a) is scaled by the wire radius. (a) Predictions when the magnetic field and fluid flow are perpendicular, as is the case for our apparatus and experiments. (b) Predictions when the magnetic field and fluid flow are parallel (and opposite).

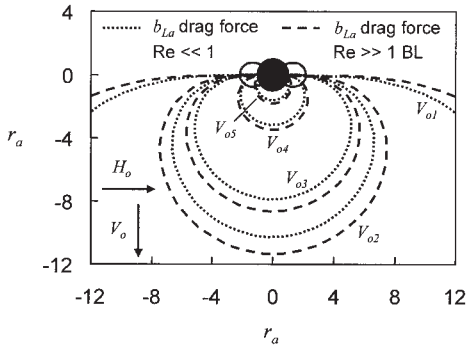

Figure 6. Comparison of model predictions with different velocity profile solutions.

The dashed lines represent the drag force buildup limit calculated using Fletcher's high Reynolds number flow solution modified with a boundary layer (BL) (Fletcher, 1991). The dotted lines represent our predictions using the low Reynolds number flow solution that more accurately describes flow near the buildup interface (Eqs. 2–4). The diffusion buildup limit is not affected because it represents nanoparticle buildup in a stagnant fluid.

Fletcher's use of a high Reynolds number flow solution (a nonphysical situation in this case) coupled with a boundary layer solution around the solid buildup. Figure 6 shows that Fletcher's boundary layer method, modified for our model conditions (perpendicular flow and field, particle superparamagnetism, and presence of a nonmagnetic shell), predicts a drag force buildup volume that is approximately 20% larger than our prediction. However, there is little effect on the predicted transition velocity between the two regimes. One of the weaker assumptions of our model (and Fletcher's) is the assumption that the particle buildup is cylindrical around the wire, which is clearly not supported by the final predictions that show highly asymmetric particle buildup lobes. In addition, a significant drag force may be exerted on the nanoparticle buildup and this would be sure to have an effect on the buildup profiles. Nevertheless, the prediction of the transition velocity is in remarkable agreement with experimental observations.

The effect of particle size on HGMS capture efficiency can be assessed as a function of the fluid velocity by integrating the common area inside both the diffusion and drag force limits (not including the wire) for particles with different magnetite core diameters. The results for a fixed n_s/n_o ratio of 24.0 and polymer shell thickness of 9.4 nm are shown in Figure 7a, where the total static buildup volume has been normalized by the wire volume. The effect of the flow velocity is seen to be qualitatively similar for particles of different core diameters, although there may be a small decrease in the transition velocity at which particle collection goes from being entirely diffusion limited to being primarily drag force limited as the core size increases. Figure 7b illustrates the shape of the static buildup of nanoparticles as V_o approaches zero for various core diameters, which in this limit is defined by the lower halves of the two diffusion-limited lobes. The total static buildup volume increases dramatically with increasing core size, reflecting the strong dependence of the magnetic force on particle volume. For small particles with a 4-nm core diameter, the dimensionless buildup limit is less than unity for all angles, which has no physical significance and implies that no static buildup is possible for particles of this size. By setting $b_{La} = 1$ at $\theta = 0$, we found that the minimum particle core diameter that can form a static buildup is 4.5 nm, which is similar to the result calculated by Takayasu et al. (1983).

Dynamic light scattering (Figure 3c) indicates that approximately 10% of the particles are present as aggregates with a diameter of 60–125 nm. To calculate the static buildup volumes of these aggregates around the wire, we assumed that they were composed of individual particles with a core diameter of 7.5 nm and total diameter of 26 nm. The dimensionless ratio of the magnetic force to the diffusive force for dense aggregates of individual particles that maintain the same volume fraction of magnetite as the individuals is given by

$$K_{md,agg} = NK_{md,ind} \tag{29}$$

where N is the number of particles in the aggregate, each with $K_{md,ind}$. The dimensionless ratio of the magnetic force to the fluid drag force for dense aggregates of individual particles can be expressed as

$$K_{mv,agg} = NK_{mv,ind}\frac{R_{shell}^2}{R_{agg}^2} \tag{30}$$

where N is the number of individual particles with $K_{mv,ind}$ and R_{shell} in aggregates of radius R_{agg}. The total static buildup

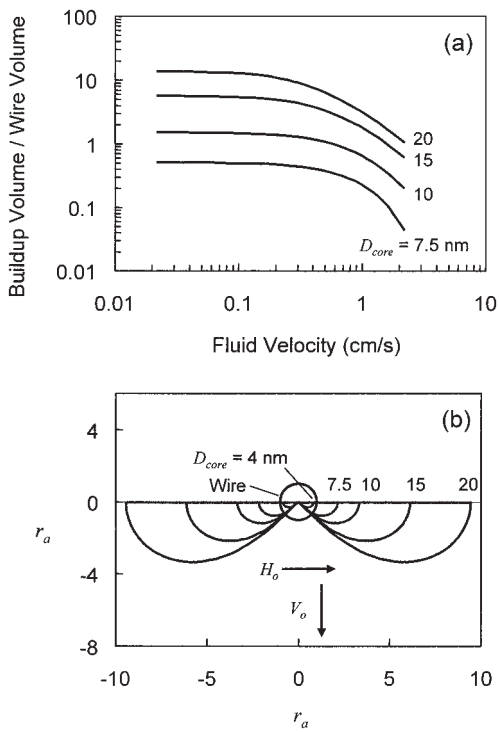

Figure 7. Effect of the core size on the static buildup volume for polymer-coated nanoparticles.

(a) The calculated volume of the static buildup limit (normalized by the wire volume) is plotted against the flow velocity (V_o). (b) The static buildup limit for different core sizes for the case when $V_o \rightarrow 0$ (but remains positive). In all calculations, n_s/n_o and the polymer shell thickness were fixed at 24 and 9.4 nm, respectively, for the purposes of comparison.

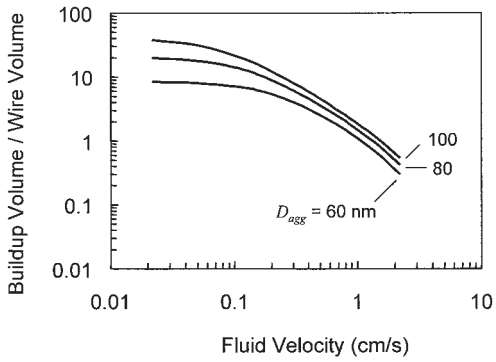

Figure 8. Effect of flow velocity on the static buildup volume of aggregates of the polymer-coated nanoparticles.

The aggregates were assumed to be composed of average nanoparticles (Figure 3d) that maintained the same volume fraction of magnetite as the individuals. n_s/n_o was fixed at 24.0 for the purposes of comparison.

volume for aggregates of different diameter as a function of the flow velocity is shown in Figure 8. The static buildup volume increases with increasing aggregate diameter in a manner similar to that of individual particles. However, the transition velocity is approximately an order of magnitude lower than that for individual particles, given that the diffusion buildup limit depends on $K_{md,agg}$, which scales directly with the number of particles in the aggregates, whereas the azimuthal buildup limit depends on $K_{mv,agg}$, which increases at a much slower rate because of the R_{shell}^2/R_{agg}^2 factor in Eq. 30. The qualitative shapes of the aggregate buildups as $V_o \rightarrow 0$ are essentially the same as those for the individual nanoparticles shown in Figure 7b.

The effect of particle size on HGMS capture was determined by magnetic chromatography experiments in which a pulse of 0.5 wt % magnetic fluid was injected into the column directly above the packing while water was passed continuously through the column. The column effluent was monitored for particle concentration and size. The flow velocity of the water (0.1 cm/s) was sufficiently low that nanoparticle diffusion was the primary mechanism opposing capture for all particles and aggregates. With the magnet off, a sharp breakthrough of particles in the column effluent with a mean residence time, t_m, of 4.1 min was observed, with a small amount of variance attributed to axial dispersion or channeling, as shown by the dashed line in Figure 9.

The particle concentration and hydrodynamic diameter in the column effluent when the magnet was operated at its maximum field strength of 1.3 T are shown as a function of residence time in Figure 9. With the magnet on, the breakthrough of particles was only slightly delayed compared to that when no field was applied, in that the maximum effluent concentration occurred at only 1.6 residence times. The number-average hydrodynamic diameter of the earliest particles to pass through the column was only 10 nm, which is significantly smaller than the initial number-average diameter (26 nm). This result is consistent with batch-filtration data (Moeser et al., 2002), which showed that the smallest particles were the least attracted to the packing material. After the smallest particles were eluted, a continuous decrease in particle concentration was observed in the effluent over the next eight residence times, as average-sized particles that were significantly hindered by the magnetic field were washed from the column until the effluent was essentially free of particles. This particle bleeding is a direct consequence of the enhanced diffusional flux away from the buildup region as the bulk particle concentration n_o is reduced, and the size of this static buildup region decreases with decreasing n_o, as predicted by Eq. 24. The magnet was then deactivated, at which point seemingly permanently trapped particles eluted from the column. This peak was observed regardless of the time between injection and deactivation of the magnet.

The number-average hydrodynamic diameter of the permanently trapped particles was 51 nm, which not only is much larger than the initial average, but also larger than any particles in the initial number-average distribution shown in Figure 3c. These permanently trapped particles are probably the 60- to 125-nm aggregates present in the volume-average distribution from DLS. On halving the concentration of the injected magnetic fluid, the size of the permanently trapped peak was also halved (data not shown), suggesting that these particles are not trapped in a limited number of sites on the packing material. The volume-average diameter of the permanently trapped particles was 94 nm, which is consistent with the size of the aggregates in Figure 3c. The smaller number-average diameter (51 nm) may be a result of some individual particles retained with the aggregates that significantly bias the number-average diameter. The fraction of particles trapped permanently (14% by volume) was consistent with the volume fraction of particles present as aggregates as determined by DLS (11%), suggesting that only the aggregates could be permanently trapped, whereas individual particles were merely hindered in their transport through the HGMS column by the magnetized wires. These permanently trapped particles do not bleed off during the timescale of the experiment because of the stronger magnetic

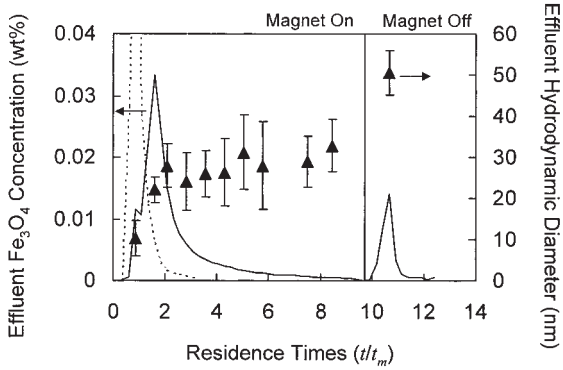

Figure 9. Magnetic chromatography of the polymer-coated magnetic nanoparticles, in which 0.5 mL of 0.5 wt % magnetic fluid was injected into the column directly above the packing material while water was passed continuously at 0.1 cm/s.

The dashed line shows the concentration of particles in the effluent as a function of time (normalized by the mean residence time) when the magnet is off, whereas the solid line shows the concentration of particles in the effluent when the magnet is operated at its maximum field strength (1.3 T). The triangles represent the number-average hydrodynamic diameter of particles in the effluent during the run with the magnet on.

forces (relative to those acting on the smaller particles) opposing the diffusional tendency for the captured particles to move away from the buildup regions on the wire.

The magnetic chromatography data indicate that average sized particles are not captured permanently in the column. Thus, the high capture efficiencies (~90–98%) observed in our batch HGMS filtrations (Moeser et al., 2002) are simply the result of a diffusional equilibrium between the static buildup zones and the bulk suspension surrounding these regions, as mediated by the magnetic forces acting on the particles. It has been noted that the feed concentration has no effect on the capture efficiency in a batch process (Moeser et al., 2002), which can be attributed to the fact that the total number of particles captured in the static buildup region will be larger the higher the bulk concentration n_o. Thus, with increasing feed concentration, both a larger buildup region and a larger residual bulk concentration of particles are obtained, constrained by overall material balances that dictate that the *fraction* of particles captured will be independent of the feed concentration; this behavior mirrors that of adsorption processes that are characterized by linear adsorption isotherms. The fraction of particles captured will depend on their size and their magnetic properties, which points to the need for optimization of these properties to enhance the utility of these tailored magnetic nanoparticles in chemical processing applications.

The calculated static buildup volumes shown in Figures 7 and 8 illustrate the different behavior of individual particles and aggregates in the HGMS column. The smallest particles in the distribution (<4.5 nm core diameter) cannot form a static buildup on the wires and so they are barely affected by the magnetic field. The average and larger-sized individual particles do form a static buildup, but upstream water washes out the bulk liquid (outside of the buildup volume), resulting in a slow erosion of the particles as a result of the diffusion equilibrium. We hypothesize that permanent capture in the HGMS column can occur only if the limiting static buildup volume is sufficiently large that it occupies the entire void space in the column. In this case, any particle entering the column would be subjected to a magnetic force sufficient to overcome the dynamic equilibrium between particles trapped in the buildup volume and those in the outside fluid. This assumption is, of course, an approximation because half the volume around a single isolated wire is predicted not to be active in trapping the particles. Overlapping of buildup regions of adjacent wires cannot be ruled out, however, in which case a larger fraction of the volume of a densely packed column can be expected to contribute to the capture of the particles. Figure 10 illustrates the static buildup volume for both individual particles and aggregates in a purely diffusion-limited case ($V_o \rightarrow 0$). Note that for individual particles we plot against the core diameter because, in the diffusion limit, the buildup volume is essentially independent of the shell thickness. The buildup volume of the aggregates increases more slowly with diameter, given that they contain less than 3 vol % magnetite because of the large polymer shell around the particles. The void volume is represented as the horizontal dashed line, calculated from the 13.7 vol % packing fraction.

We accounted for the fact that the wire orientation in the HGMS column is essentially random in the plane perpendicular to the flow direction by assuming that approximately half of the wires are oriented parallel to the applied field, inducing no

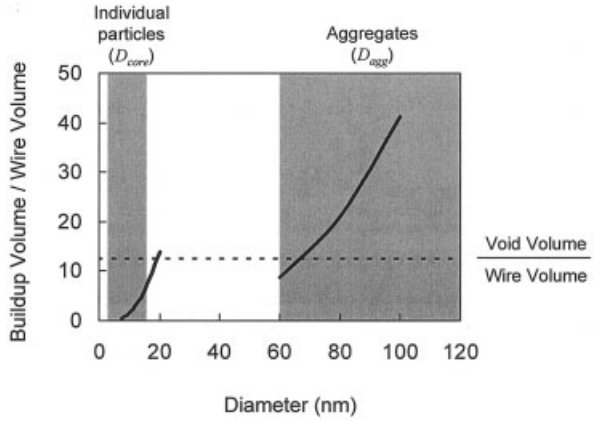

Figure 10. Static buildup volume of individual polymer-coated nanoparticles and particle aggregates compared to the void volume of the column.

The solid lines represent the calculated limit of static nanoparticle buildup as $V_o \rightarrow 0$ (representative of the conditions used in our magnetic chromatography experiments) for individual particles of varying core diameter (D_{core}) and aggregates of varying total diameter (D_{agg}). The shaded regions represent the measured size range of the individual particles and the aggregates. The dashed line shows the void volume of the column. Permanent capture of particles or aggregates should occur when the static buildup volume of the particles around the wires exceeds the void volume of the column.

magnetic field gradients in the liquid as discussed above; other assumptions of the "active" fraction of wires could be made, but any such reasonable assumptions would not affect the overall conclusions, and the quantitative consequences would not be significant at this level of analysis, that is, would affect the predicted cutoff diameters only slightly. If these wires are considered to be equivalent to dead space, the volume fraction of active wires (with the geometry shown in Figure 2) is closer to 6.9 vol %, which results in a normalized void volume of 12.6. All of the individual nanoparticles ($3 < D_{core} < 15$ nm) have a static buildup volume that occupies less than the void volume, so they should eventually be washed from the column by upstream liquid. The buildup volume of the aggregates, however, occupies all of the void space when the diameter exceeds approximately 70 nm. Because the aggregates are 60–125 nm in diameter, the theoretical predictions are consistent with our experimental observations that aggregates are captured permanently during magnetic chromatography.

For permanent capture of the individual nanoparticles in our HGMS column to be feasible, the particles would require a larger diffusion-limited buildup volume, determined by the value of K_{md}. Equation 27 shows that for a particle with a given core radius, the only practical methods for increasing this ratio are by increasing the magnetization of either the packing material or the particle core, or both. As shown in Figure 3b, at the applied field strength of 1.3 T, the particles are magnetically saturated and increases in the applied magnetic field will not increase M_{core}. Likewise, the stainless steel packing is saturated at 1.3 T (Gerber and Birss, 1983), and HGMS performance cannot be improved by further increases in the applied field (Takayasu et al., 1983). One possibility would be to use nanoparticles (or wires) with a higher saturation magnetization, such as cobalt; however, cobalt is less stable to oxidation and

more costly than magnetite and stainless steel. Another strategy would be to increase the volume fraction of "active" wires in the column by using a structured packing. In essence, though, for HGMS to be a practical process, it would be necessary to form clusters or aggregates of the individual nanoparticles that can be more readily captured by HGMS.

HGMS of phospholipid-coated nanoparticles

Magnetite nanoparticles coated with a surfactant-phospholipid bilayer for the selective binding of proteins based on electrostatic charge have recently been discussed (Bucak et al., 2003). In contrast to the polymer-coated particles discussed above, the phospholipid-coated nanoparticles were captured successfully in preliminary bench-scale studies (Bucak et al., 2003). The core size distribution and magnetization response of these phospholipid-coated particles were essentially identical to those of the polymer-coated nanoparticles as presented in Figures 3a and b. The surfactant-phospholipid bilayer should form a 4-nm-thick layer on the surface, but DLS results showed that these nanoparticles exist as small aggregates in the 25- to 50-nm size range, with a number-average diameter of 32 nm (Bucak et al., 2003). We estimate that an average aggregate would consist of approximately nine individual particles if the magnetite volume fraction in the aggregate is the same as that for individual particles. Roughly 1–2 wt % of the particles exist as much larger aggregates and can be ignored for our purposes (Bucak et al., 2003).

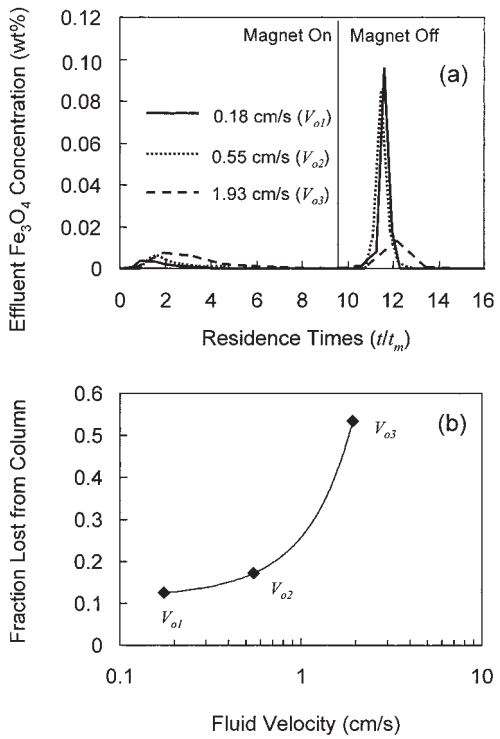

Figure 11. (a) Magnetic chromatography of the phospholipid-coated magnetic nanoparticles, in which 0.5 mL of 1.36 wt % magnetic fluid was injected into the column directly above the packing material while water was passed continuously at various flow velocities [the lines represent the concentration of particles in the effluent as a function of time (normalized by the mean residence time)]; (b) the calculated fraction of particles lost from the column.

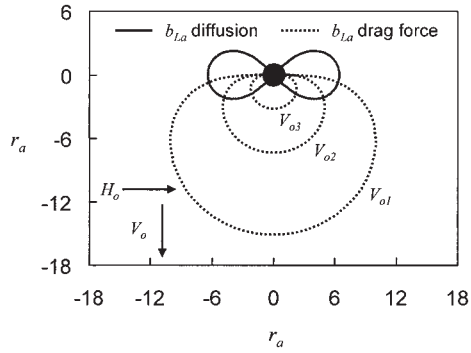

Figure 12. Predicted diffusion (solid line) and drag force (dotted line) limits of static buildup for the phospholipid-coated nanoparticle aggregates.

The actual limit of static buildup at a given flow velocity is defined by the intersection of the areas inside both curves.

Figure 11a shows the results of a magnetic chromatography experiment in which a pulse of the phospholipid magnetic fluid (1.36 wt % Fe_3O_4) was injected into the column while water was passed at three different velocities. In contrast to the polymer-coated nanoparticles, a significant fraction of the particles was trapped permanently in all cases regardless of the flow velocity, suggesting that HGMS can be applied successfully to these particles after removing the small fraction that cannot be captured (Bucak et al., 2003). The fraction of escaping particles increased as the flow velocity increased, as shown in Figure 11b.

Figure 12 shows the limit of static buildup for the three different velocities, assuming the nanoparticles were present as dense 32-nm-diameter aggregates of particles with a 7.5-nm magnetite core and a 15.5-nm total shell diameter (that maintain the same volume fraction of magnetite as the individual particles), with an n_s/n_o ratio of 22.5. It is clear from the profiles that the magnetic chromatography experiments at all three velocities were conducted in the fluid drag force-limited regime because the limit of static buildup increases in volume as the velocity decreases. This trend is consistent with the magnetic chromatography results shown in Figure 11, in which greater capture efficiency was obtained at the lower flow velocities. The transition velocity below which HGMS of the phospholipid-coated particles becomes diffusion-controlled is close to V_{o1} (0.18 cm/s), given that the drag force buildup limit has nearly reached the diffusion limit, suggesting that there would be little further benefit in reducing the velocity below 0.18 cm/s.

In the diffusion-controlled regime, the effect of particle size on capture is determined purely by the diffusion buildup limit, as shown in Figure 13 for phospholipid-coated aggregates of varying total diameter. The aggregate buildup volume, as $V_o \rightarrow 0$ (solid line), exceeds the total void space (dashed line) in the column, which is indicative of permanent capture, when the aggregate diameter exceeds approximately 40 nm. DLS

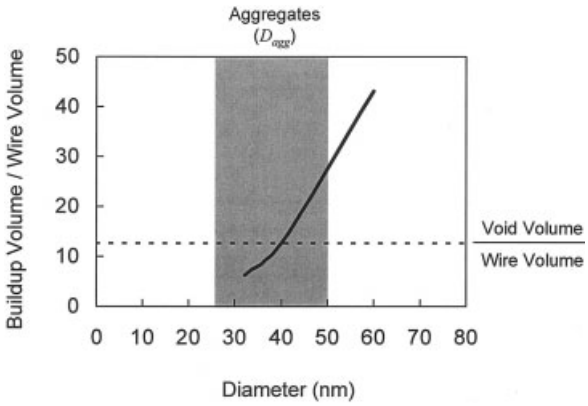

Figure 13. Static buildup volume of the phospholipid-coated particle aggregates compared to the void volume of the column.

The solid line represents the calculated limit of static nanoparticle buildup as $V_o \rightarrow 0$ for aggregates of varying total diameter (D_{agg}), whereas the shaded region represents the measured size range of the aggregates. The dashed line shows the void volume of the column.

showed that these aggregates span a range from 25 to 50 nm in diameter (Bucak et al., 2003), which explains why some aggregates are permanently captured, whereas others are lost from the column. Our theoretical prediction of the minimum aggregate diameter for permanent capture (40 nm) is likely too high, given that magnetic chromatography experiments (Figure 11b) showed that only 13% of the particles were lost from the filter at a low flow velocity, which DLS results suggest should occur if the cutoff diameter were 28 nm (that is, 13% of the aggregates are less than 28 nm in diameter) (Bucak et al., 2003). Our overprediction of the minimum aggregate diameter for capture could be a result of either the aggregate being more densely packed than we assumed, which could occur if the phospholipid layer coated the aggregate instead of individual particles, or an underestimation of the fraction of "active" wires in determining the buildup volume to wire volume ratio.

Conclusions

We have examined the feasibility of using high-gradient magnetic separation to remove magnetic nanoparticles from water. We examined both polymer-coated magnetic nanoparticles for organic removal from water and phospholipid-coated particles for protein separation. These tailored nanoparticles have potential advantages over traditional separation methods because of their small particle size (Bucak et al., 2003; Moeser et al., 2002). The polymer-coated magnetic nanoparticles for the removal of organic compounds from water consisted of a magnetite core of 7.5-nm median diameter surrounded by a hydrated polymer coating of 9.4-nm thickness; a small fraction (11–14%) of the particles was present as 60- to 125-nm aggregates. We observed that, even when the liquid was passed at a low flow velocity, the individual nanoparticles in these magnetic fluids could not be trapped permanently by HGMS, whereas the aggregates could be captured permanently. HGMS was much more successful at capturing the phospholipid-coated particles, which consisted of 7.5-nm magnetite particles that formed 25- to 50-nm aggregates. Approximately 87% of these aggregates were permanently trapped when the liquid was passed at a low flow velocity. After removing the small fraction that was not permanently captured by the magnet, the remaining aggregates could be captured effectively and would be suitable for use in a traditional HGMS process.

We developed a theory, based on the earlier work of Fletcher (1991), but with several modifications, that described the static buildup of nanoparticles around the collection wires for the geometry of our HGMS column. This theory showed that magnetic filtration can be divided into two regimes: a high flow velocity regime in which fluid drag is the primary force opposing capture and a low flow velocity regime in which diffusion acts primarily against particle capture. The transition velocity between these two regimes has been determined theoretically and experimentally for the nanoparticle systems studied here, with good agreement between theory and experiment. Theoretical estimates showed that individual Fe_3O_4 nanoparticles with a core diameter less than 20 nm cannot be captured permanently in our HGMS column. Aggregates can be captured permanently because the entire void space of the column is inside the limit of static buildup of the aggregates around a collection wire. The minimum aggregate size for permanent capture was calculated to be 40 nm for the phospholipid-coated particles and 70 nm for the polymer-coated particles; this difference is attributed to the higher volume fraction of magnetite in the phospholipid aggregates.

The phospholipid-coated particles constitute a good candidate for magnetic separation in their current form because they consist primarily of aggregates that were captured permanently in the HGMS column. The polymer-coated particles must be modified before they can be used in a traditional HGMS separation process, in that only a small fraction is present as aggregates. Several possibilities exist for improving the magnetic filtration of these magnetic fluids. First, traditional HGMS could be adapted by using magnetic fields to push the nanoparticles in a different direction than the flow of the dispersion medium. There is some evidence to suggest that such field-flow fractionation techniques are more successful for nanoparticles than conventional HGMS (Tsukamoto et al., 1995), although these processes have a much lower capacity. A second possibility is to adapt the nanoparticles for easier capture by conventional HGMS. The development of particles that can form small clusters while maintaining large surface areas and high capacities for the target organics should lead to magnetic fluids with the appropriate properties for use in practical separation processes. This approach is currently an area of active research.

Acknowledgments

This work was supported by the National Science Foundation (CTS-9817221) and the Singapore-MIT Alliance. G. Moeser thanks the Eastman Kodak Company for Kodak Fellowship support. We thank Seyda Bucak and Deverraux Jones (MIT) for supplying data from their experiments with the phospholipid-coated nanoparticles.

Literature Cited

Bucak, S., D. J. Jones, P. E. Laibinis, and T. A. Hatton, "Protein Separations Using Colloidal Magnetic Nanoparticles," *Biotechnol. Prog.*, **19**, 477 (2003).

Buchholz, B. A., L. Nunez, and G. F. Vandegrift, "Radiolysis and Hydrolysis of Magnetically Assisted Chemical Separation Particles," *Sep. Sci. Technol.*, **31**, 1933 (1996).

Cotten, G. B., and H. B. Eldredge, "Nanolevel Magnetic Separation Model Considering Flow Limitations," *Sep. Sci. Technol.*, **37**, 3755 (2002).
Ebner, A. D., and J. A. Ritter, "New Correlation for the Capture Cross Section in High-Gradient Magnetic Separation," *AIChE J.*, **47**, 303 (2001).
Ebner, A. D., J. A. Ritter, and H. J. Ploehn, "Feasibility and Limitations of Nanolevel High Gradient Magnetic Separation," *Sep. Purif. Technol.*, **11**, 199 (1997).
Feltin, N., and M. P. Pileni, "New Technique for Synthesizing Iron Ferrite Magnetic Nanosized Particles," *Langmuir*, **13**, 3927 (1997).
Fletcher, D., "Fine Particle High Gradient Magnetic Entrapment," *IEEE Trans. Magn.*, **27**, 3655 (1991).
Gerber, R., and R. R. Birss, *High Gradient Magnetic Separation*, Research Studies Press, London (1983).
Gerber, R., M. Takayasu, and F. J. Friedlaender, "Generalization of HGMS Theory: The Capture of Ultra-fine Particles," *IEEE Trans. Magn.*, **19**, 2115 (1983).
Hubbuch, J. J., and O. R. T. Thomas, "High-Gradient Magnetic Affinity Separation of Trypsin from Porcine Pancreatin," *Biotechnol. Bioeng.*, **79**, 301 (2002).
Kaminski, M. D., and L. Nunez, "Extractant-Coated Magnetic Particles for Cobalt and Nickel Recovery from Acidic Solution," *J. Magn. Magn. Mater.*, **194**, 31 (1999).
Leun, D., and A. K. Sengupta, "Preparation and Characterization of Magnetically Active Polymeric Particles (MAPPs) for Complex Environmental Separations," *Environ. Sci. Technol.*, **34**, 3276 (2000).
Moeser, G. D., "Colloidal Magnetic Fluids as Extractants for Chemical Processing Applications," PhD Thesis, Massachusetts Institute of Technology, Cambridge, MA (2003).
Moeser, G. D., K. A. Roach, W. H. Green, P. E. Laibinis, and T. A. Hatton, "Water-Based Magnetic Fluids as Extractants for Synthetic Organic Compounds," *Ind. Eng. Chem. Res.*, **41**, 4739 (2002).
Moyer, C., M. Natenapit, and S. Arajs, "Magnetic Filtration of Particles in Laminar-Flow through a Bed of Spheres," *J. Magn. Magn. Mater.*, **44**, 99 (1984).
Rosensweig, R. E., *Ferrohydrodynamics*, Dover Publications, Mineola, NY (1985).
Safarik, I., "Removal of Organic Polycyclic Compounds from Water Solutions with a Magnetic Chitosan Based Sorbent Bearing Copper Phthalocyanine Dye," *Water Res.*, **29**, 101 (1995).
Safarik, I., and M. Safarikova, "Use of Magnetic Techniques for the Isolation of Cells," *J. Chromatogr. B*, **722**, 33 (1999).
Shen, L., P. E. Laibinis, and T. A. Hatton, "Bilayer Surfactant Stabilized Magnetic Fluids: Synthesis and Interactions at Interfaces," *Langmuir*, **15**, 447 (1999).
Takayasu, M., R. Gerber, and F. J. Friedlaender, "Magnetic Separation of Submicron Particles," *IEEE Trans Magn.*, **19**, 2112 (1983).
Tsukamoto, O., T. Ohizumi, T. Ohara, S. Mori, and Y. Wada, "Feasibility Study on Separation of Several Tens Nanometer-Scale Particles by Magnetic Field-Flow-Fractionation Technique Using Superconducting Magnet," *IEEE Trans. Appl. Supercond.*, **5**, 311 (1995).
Wangsness, R. K., *Electromagnetic Fields*, Wiley, New York (1979).
Ying, T. Y., S. Yiacoumi, and C. Tsouris, "High-Gradient Magnetically Seeded Filtration," *Chem. Eng. Sci.*, **55**, 1101 (2000).
Yoe, J. H., and L. Jones, "Colorimetric Determination of Iron with Disodium-1,2-dihydroxybenzene-3,5-disulfonate," *Ind. Eng. Chem.*, **16**, 111 (1944).

Manuscript received Aug, 18, 2003, and revision received Mar. 16, 2004.